




# Internal Tides Responsible for Lithogenic Inputs Along the Iberian Continental Slope

Simon Barbot<sup>1</sup> , Marion Lagarde<sup>1</sup> , Florent Lyard<sup>1</sup> , Patrick Marsaleix<sup>1</sup> , Pascale Lherminier<sup>2</sup> , and Catherine Jeandel<sup>1</sup> 

<sup>1</sup>LEGOS, Université de Toulouse, CNES, CNRS, IRD, UPS, Toulouse, France, <sup>2</sup>LOPS, Ifremer, University Brest, CNRS, IRD, IUEM, Plouzané, France

### Key Points:

- Sites of high bottom tidal velocity along the Iberian continental slope were identified using a semi-realistic internal tides model
- Sediment resuspension was confirmed on five sites based on earlier sediment surveys and Shields criterion threshold
- Particle trajectories were proposed based on circulation modeling to improve the interpretation of geochemical tracers measurements

### Supporting Information:

Supporting Information may be found in the online version of this article.

### Correspondence to:

S. Barbot,  
[simon.barbot@legos.obs-mip.fr](mailto:simon.barbot@legos.obs-mip.fr)

### Citation:

Barbot, S., Lagarde, M., Lyard, F., Marsaleix, P., Lherminier, P., & Jeandel, C. (2022). Internal tides responsible for lithogenic inputs along the Iberian continental slope. *Journal of Geophysical Research: Oceans*, 127, e2022JC018816. <https://doi.org/10.1029/2022JC018816>

Received 3 MAY 2022

Accepted 9 SEP 2022

### Author Contributions:

**Conceptualization:** Simon Barbot, Marion Lagarde, Florent Lyard, Catherine Jeandel

**Data curation:** Marion Lagarde, Patrick Marsaleix, Pascale Lherminier, Catherine Jeandel

**Formal analysis:** Simon Barbot

**Funding acquisition:** Florent Lyard, Catherine Jeandel

**Investigation:** Simon Barbot, Marion Lagarde

**Methodology:** Simon Barbot, Marion Lagarde, Florent Lyard, Patrick Marsaleix

**Project Administration:** Florent Lyard, Pascale Lherminier, Catherine Jeandel

**Resources:** Simon Barbot, Marion Lagarde

**Software:** Florent Lyard, Patrick Marsaleix

**Abstract** This study proposes new insights for the interpretation of GEOVIDE particle measurements. Potential resuspension sites due to internal tides (ITs) have been identified along the western Iberian shelf slope using a tidal regional model. Iberian shelf is mainly a source of lithogenic material whereas Galicia Bank is a source of biogenic matter. The potential pathways for particles from the resuspension sites toward the GEOVIDE stations are identified using IBIRYS reanalysis to infer their transport by the ocean circulation. It appears that each station is influenced by a specific pathway and mixed particles from several resuspension sites. This methodology reveals that the criticality of the bathymetry slope, commonly used to track resuspension sites from internal waves, is not sufficient to investigate ITs. An explicit resolution of ITs using a numerical tidal model is required for an exhaustive identification of the resuspension sites.

**Plain Language Summary** Internal tides (ITs) are waves with a tidal period generated when tides cross a steep slope of the sea floor. ITs then propagate in every stratified layer of the open ocean over hundreds to thousands of kilometers. The encounter of ITs with underwater relief, either at the generation site or after propagation, results in high bottom friction that enhances sediment resuspension. Evidence of lithogenic particles was found at various depths during the GEOVIDE cruise, from the Iberian continental slope to thousands of kilometers away. The present study identifies the sites where ITs are responsible for sediment resuspension. Additionally, the oceanic circulation is investigated to establish the trajectories of the resuspended sediment that could explain the GEOVIDE measurements.

## 1. Introduction

The GEOVIDE cruise took place in May/June 2014 onboard the R/V “Pourquoi Pas ?” between Lisbon, Greenland, and Newfoundland. This cruise was part of the GEOTRACES program, an international cooperation that aims to study trace elements and their isotopes distributions and cycles in the global ocean. Suspended particles were sampled between the surface and 1,000 m at several stations by in situ sea water filtration. They were found to have higher Rare Earth Elements (REEs) and iron concentrations closer to the Iberian margin and to contain 40%–100% of lithogenic material (Gourain et al., 2019; Lagarde et al., 2020). Additionally, a continuous propagation of intermediate nepheloid layers was observed as far as 2,000 km away, following isopycnal layers at the following depths: 180, 220, 500, and 800 m (corresponding to potential density anomalies  $\sigma = 27.00, 27.05, 27.18, \text{ and } 27.39 \text{ kg.m}^{-3}$  respectively, Figure 1b, Lagarde et al., 2020). These results suggest intense resuspension along the Iberian continental slope, followed by a transport mechanism allowing the sediment to reach the middle of the Atlantic Ocean as hypothesized by Lagarde et al. (2020). Furthermore, the significant resuspension of particles of strict lithogenic origin leads to the formation of intermediate nepheloid layers when the sediment propagates off-shelf (McCave & Hall, 2002). The presence of nepheloid layers is effectively observed at all depths along the GEOVIDE section, except at 700 m at station 1 (nearest station to the shelf).

The Iberian Peninsula has benefited from a wide coverage of sediment sampling, starting with the surveys of the Dias and Nittrouer (1984), then the OMEX I project and finally the OMEX II-II program. Thanks to the numerous publications of these projects and its database, it is possible to have a complete description of the sediment: grain size spectrum, density, and nature. These three properties are necessary to study the resuspension of sediments because a heavier sediment will require a faster current for its resuspension. The nature of the sediment defines whether the sediment was created from submerged organisms (biogenic) or from erosion of the continental crust

**Supervision:** Simon Barbot, Marion Lagarde, Florent Lyard  
**Validation:** Simon Barbot, Florent Lyard, Patrick Marsaleix, Pascale Lherminier  
**Visualization:** Simon Barbot  
**Writing – original draft:** Simon Barbot  
**Writing – review & editing:** Simon Barbot, Marion Lagarde, Florent Lyard, Patrick Marsaleix, Pascale Lherminier, Catherine Jeandel

(lithogenic). Knowledge of the nature of the resuspended sediment is then mandatory to link the resuspension sites to the GEOVIDE measurements (Figure 1) and better interpret them.

The contribution of internal tides (ITs) and internal solitary waves (ISWs) to sediment resuspension at the margins was demonstrated by lab experiments (Cacchione, 1970), in situ measurements (Huthnance, 1989; Jia et al., 2019), and more recently by numerical modeling (Masunaga et al., 2020). Boegman and Stastna (2019) illustrated all the observations of sediment resuspension and transport due to ISWs measurements until then and explained the mechanisms of sediment resuspension by internal waves. Contrasting with the oceanic circulation that transports particles along isopycnals, the turbulence associated with the shoaling of internal waves over the topography enables particles to be transported across isopycnals (Masunaga et al., 2017). ITs and ISWs are generated by distinct forcing that develops a perturbation of the stratification of the water column. They propagate with strong vertical displacements of the isopycnals and enhanced currents.

ISWs have been proposed to explain sediment resuspension along the Iberian shelf (Dias et al., 2002; McCave & Hall, 2002; Oliveira et al., 2002; Quaresma et al., 2007; Schmidt et al., 2002; Van Weering et al., 2002). ISWs are generated by the wind over a stratified upper ocean or by the tides in a shallow stratified ocean such as a river plume. They can have a large vertical amplitude (<200 m) and enhanced currents (<2 m.s<sup>-1</sup>) but mainly propagate in the first 300 m along the pycnocline (Marin, 2011); therefore, they cannot fully explain the GEOVIDE observations (Figure 1).

ITs have been observed along the Nazaré canyon without direct evidence of sediment resuspension (Huthnance et al., 2002). Contrary to barotropic tidal currents, which affect the entire water column with a quasi-uniform amplitude, ITs propagate across every stratified layer and the associated currents show a highly variable 3D pattern. Their internal oscillation amplitude is generally weaker than that of ISWs (<100 m and <1 m.s<sup>-1</sup>) but they are highly energetic and constantly generated with a tidal period (de Lavergne et al., 2019). IT energy propagates from IT generation sites in a specific pathway called the wave beam. Effective bottom friction effects are expected where the IT energy flux reaches the seabed, possibly in close vicinity of the generation sites (Garrett & Kunze, 2007, their Figure 8). Ribbe and Holloway (2001) showed that IT energy is most efficiently dissipated by friction when the bathymetry slope is parallel to the IT wave beam, a situation called the critical slope which leads to sediment resuspension. The criticality of a bathymetric slope depends on stratification and the tidal period. Its temporal variability is only controlled by the temporal variability of the stratification. This simple criterion is widely used in the geochemical community to identify potential resuspension sites due to the presence of ITs or ISWs at those sites (Cacchione et al., 2002; de Madron et al., 1999; Lam et al., 2020; Puig et al., 2004). ISWs are more randomly generated than ITs, so such a criterion is still valid. However, this approach gives no information on the occurrence of ITs crossing the slope.

The full signal of ITs off-shelf is not easily observed because of their short periods, 3D propagation pattern, and wavelengths of several tens of kilometers. Considering both barotropic and baroclinic tides in circulation models is likely to raise numerical difficulties, such as stability or spurious long-term erosion of the stratification due to strong currents. To date, these processes have been simulated at shelf-scale (tens to hundreds of kilometers) focusing on shallow waters but rarely at wider scales to focus on intermediate sediment resuspension and transport. Molinas et al. (2020) used a tidal regional model to investigate the IT residual currents influencing particle transport over the Amazon shelf but applied their calculation to the shelf only and did not consider the slope and the area further offshore. Masunaga et al. (2020) used a tidal regional model with idealized bathymetry coupled with a sediment model to quantify sediment resuspension and the transport of particles associated with ITs. However, their study did not compare the transport of particles due to ITs to that due to oceanic circulation.

In this context, our purpose is to investigate how ITs trigger sediment resuspension and subsequent transport, as observed along the Iberian margin. First, the 3D hydrodynamic numerical model SYMPHONIE (<https://sites.google.com/view/symphonieoceanmodel/home>). Marsaleix et al. (2008, 2019), forced solely by tides, is used to numerically investigate the bottom current speed and energy budget of ITs. This model was previously deployed in the northeast Atlantic region to study IT dynamics (Pairaud et al., 2010, 2008) and the tidal influences on river plume (Toublanc et al., 2018). The present configuration is based on a high-resolution grid (1 km in the region of interest) and a density field coherent with the GEOVIDE cruise hydrographic conditions. Second, sediment resuspension is investigated using simulated bottom friction and sediment properties. Finally, the consecutive transport of the nepheloid layers is investigated using IBIRYS12 (<https://doi.org/10.48670/moi-00029>, Iberian-Biscay-Irish

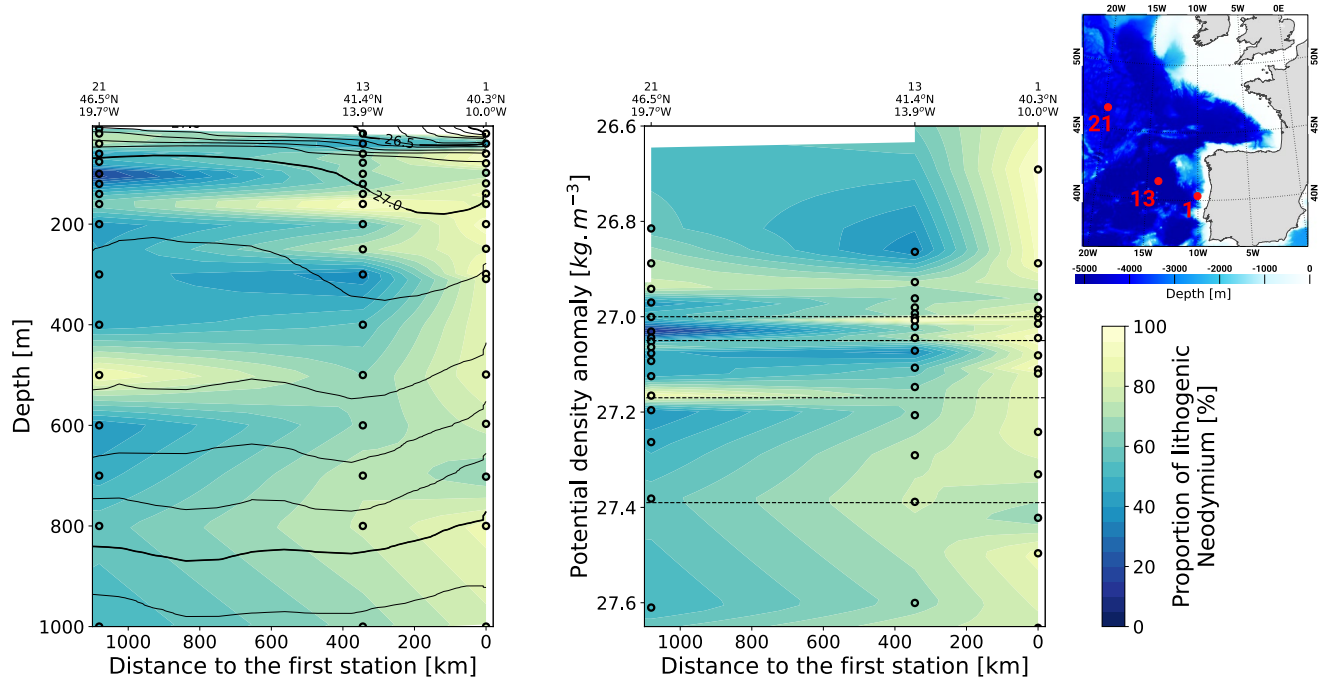


**Figure 1.** Proportion of lithogenic neodymium in suspended particles (in %) along the three first stations over (a) depth and (b) isopycnals. Data from GEOVIDE measurements (black circles) were linearly interpolated with depth (a) and density (b). The solid black lines represent isopycnals of potential density anomaly. The horizontal dashed lines correspond to the isopycnals of the observed nepheloid layers. Station numbers and locations are shown on top of section plots and on the map at the top-right. Data from Lagarde et al. (2020).

ocean Reanalysis, hereafter IBIRYS), an operational reanalysis: using 3D hydrodynamic model NEMO (Maraldi et al., 2013), historical simulations have been made using in situ measurements to regularly corrected the value of the state variables. This methodology gives realistic insight of the historical state of the ocean for the main physical component (temperature, salinity, and velocity). By exploring these processes, this study proposes a mechanistic link between the observed geochemical tracer distributions and the activity of ITs.

## 2. IT Simulation

### 2.1. SYMPHONIE Model Configuration

A regional configuration of the SYMPHONIE model, called BOBIBE (Bay of Biscay/Iberian shelf), was set up and 3D tidal simulations were carried out to quantify IT bottom currents and energy dissipation. The BOBIBE configuration uses a realistic bathymetry over a structured grid with a horizontal resolution near 1 km and with 61 vanishing quasi-sigma vertical levels (Estournel et al., 2021). Tides are forced as boundary conditions (with tidal velocity and tidal surface height) and using the astronomical potential. Tidal forcing is based on FES2014b atlas (Lyard et al., 2021) for the M2, S2, K1, and O1 tidal harmonics. These tidal harmonics are selected because they have the largest amplitudes in the studied area and can be separated by harmonic analysis over 15 days. A one-dimensional vertical density profile, representative of the GEOVIDE cruise section, is uniformly prescribed and maintained over the domain. The ocean atmosphere fluxes are disabled preventing any density-driven or wind-driven circulation in the simulation. Further details about the configuration can be found in Text S2 in Supporting Information S1.

This IT-dedicated configuration allows the development of a stable IT regime and thus provides a more precise harmonic analysis to extract ITs. The spectral properties (amplitude and phase lag) are extracted from the simulation using harmonic analysis over 1 month of simulation after 15 days of spinup. To separate the barotropic tides from ITs, the results are projected over the first 10 vertical modes based on the mean stratification after spinup. The diagnostics of IT generation and energy flux calculations are based on this modal separation of the results.

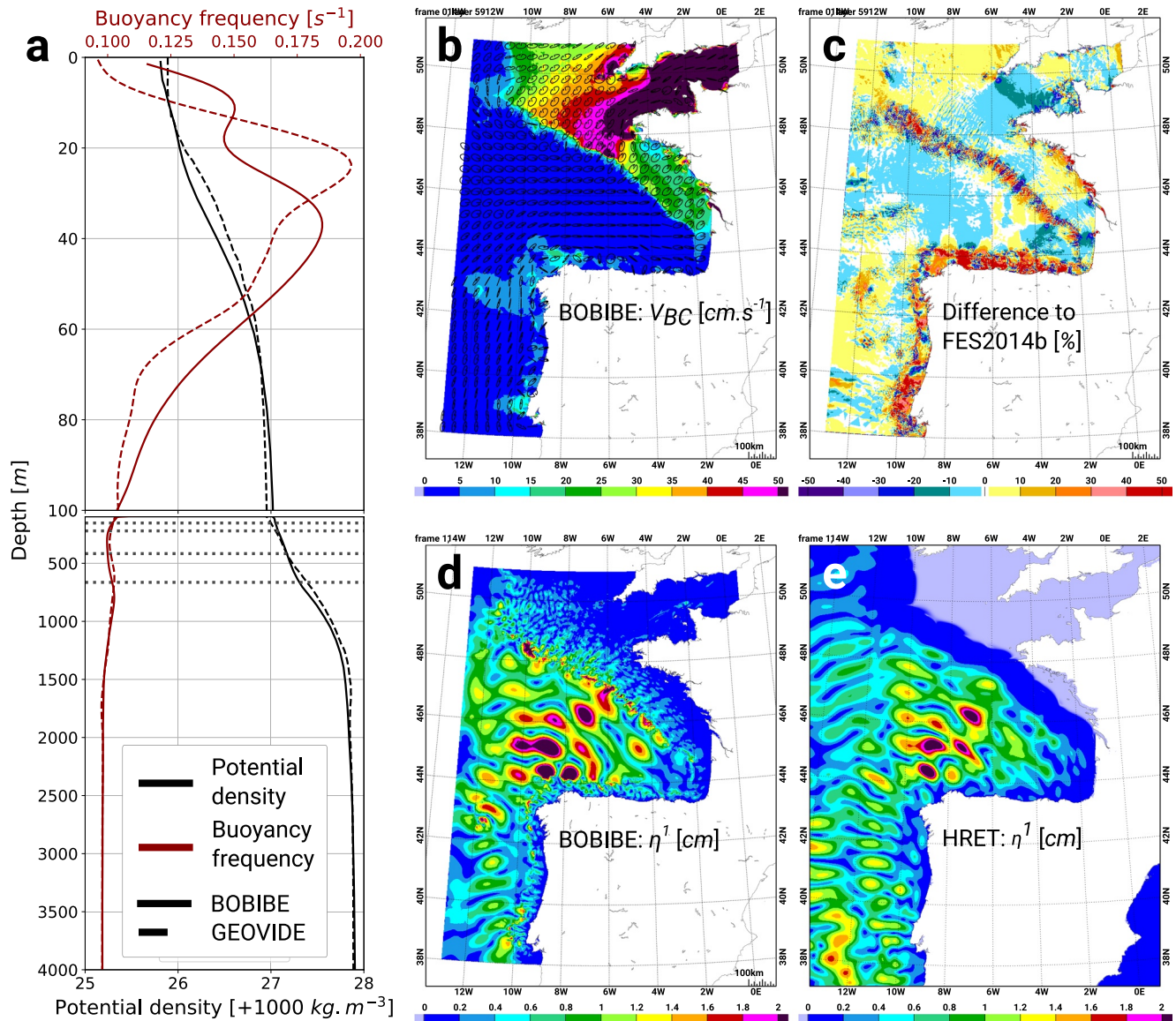


**Figure 2.** (a) Comparison of the stratification used in BOBIBE and that measured during GEOVIDE (average from the first 11 stations). (b) Amplitude of barotropic velocity for M2 in BOBIBE; and (c) difference to FES2014b atlas in proportion, the white color represents a difference within  $\pm 1\%$ . (d) Elevation amplitude of the first baroclinic mode for M2 in BOBIBE; and (e) stationary signal of ITs from HRET. The horizontal dashed lines in (a) correspond to the depths of the observed nepheloid layers.

## 2.2. Validation of the Simulation

The validation of the BOBIBE simulation focused on the stratification, barotropic velocity, and surface elevation due to ITs. The stratification is compared to that observed during GEOVIDE over the simulation area (average from the first 11 stations). Figure 2a shows that the pycnocline is located at the same depth ( $\sim 30$  m) and despite slight differences at the surface, the stratifications match.

The amplitude of the barotropic velocity was compared to the FES2014b tidal atlas. The major harmonic, M2, is presented in Figures 2b and 2c (the remaining tidal harmonics can be found in Figure S2 in Supporting Information S1). The difference is presented in proportion and the white color represents a difference within  $\pm 1\%$ . The difference between BOBIBE and FES2014b only exceeds 10% at the shelf break and over the Iberian shelf. The barotropic tide is highly sensitive to the bathymetry and energy consumption from IT generation (mostly happening at the shelf break in this area). The bathymetry is better resolved and the IT generation is better constrained

in BOBIBE than in FES2014b; therefore, the differences appear reasonable and demonstrate that the overall barotropic tides are well captured.

As explained in the introduction, the measurement of ITs is difficult, making the validation delicate. HRET, one of the best global IT data set, analyzes 20 yr of altimetric surface elevation measurements in order to extract the stationary state of ITs globally over different tidal harmonics (Zaron, 2019). The spatial sampling of long-term altimetry (1 Hz data) cannot resolve the IT higher modes, so we choose to compare HRET to the first mode of the BOBIBE simulation. The comparison with M2 is presented in Figures 2d and 2e; the remaining tidal harmonics can be found in Figure S3 in Supporting Information S1). The amplitude pattern of ITs is highly similar within the center of the Bay of Biscay but stronger over the Galicia Bank and weaker at the southwest of the domain. HRET uses the hypothesis that ITs are propagating like plane waves to better constrain IT mapping. Such hypothesis appears relevant for large shelf breaks or ridges but is inappropriate for an isolated seamount like the Galicia Bank, where IT propagation is more concentric. At the southwest of the domain, HRET seems to capture the northward ITs generated at the Gorringe Bank, which are not included in the BOBIBE domain.

### 2.3. IT Generation and Propagation

Based on the method described in Buijsman et al. (2017), IT energetics are investigated using two quantities: the energy flux ( $F_{BC}$ ) and the conversion rate (CRV). CRV corresponds to the energy of barotropic tide (BT) converted to baroclinic tide (BC) at the sea floor. Positive CVR values refer to IT generation zones, while negative values refer to a sink of IT energy. Sink zones may correspond to the shoaling of ITs over the bathymetry and could be associated with sediment resuspension. In addition, IT energy fluxes enable the tracking of IT propagation from their generation site to their sink.

$F_{BC}$  and CRV are defined by the following equations:

$$F_{BC} = \int_b^0 \nabla_h \cdot \langle p_{BC} V_{BC} \rangle dz \quad (1)$$

$$CVR = \nabla_h \cdot \langle p_{BC}^b V_{BT}^b \rangle \quad (2)$$

with  $p$  is the pressure and  $V$  is the current velocity,  $\langle \rangle$  indicates that the quantities are averaged along the considered tidal period,  $\nabla_h$  refers to the horizontal gradient and  $b$  refers to the sea floor.

Figure 3a shows the IT energy budget and identifies several generation sites with a complex energy propagation. Along the Iberian Peninsula, the major generation sites are La Coruña shelf (43°N, 9°W), the Galicia Bank (43°N, 12°W), and the Estremadura Spur shelf (39°N, 10°W). In some areas, the ITs do not propagate and sink locally (shading arrows).

As explained in the introduction, the criticality of the bathymetric slope is widely used to investigate the potential of sediment resuspension from internal waves. The criticality is expressed by the ratio of bathymetric slope over IT wave beam angle (Text S1 in Supporting Information S1), whose values of  $\sim 1$  indicate critical slopes (Figure 3b). We observe that most shelf breaks present critical slopes (from 400 to 2,000 m) that could trigger sediment resuspension. We will now compare this static methodology, only based on the bathymetry and density profile, to a more dynamical methodology involving the current velocity due to ITs.

## 3. Sediment Resuspension Triggered by ITs

### 3.1. IT Bottom Friction

To determine where ITs can trigger sediment resuspension, examining the conversion rate is not sufficient because we need to study the kinetic energy applied to the sea floor: the bottom shear stress (or bottom friction). This variable ( $\tau_b$ ) is calculated using the equation encoded in the model:

$$\tau_b = \rho V_*^2 = \rho C_D V^2 \quad (3)$$

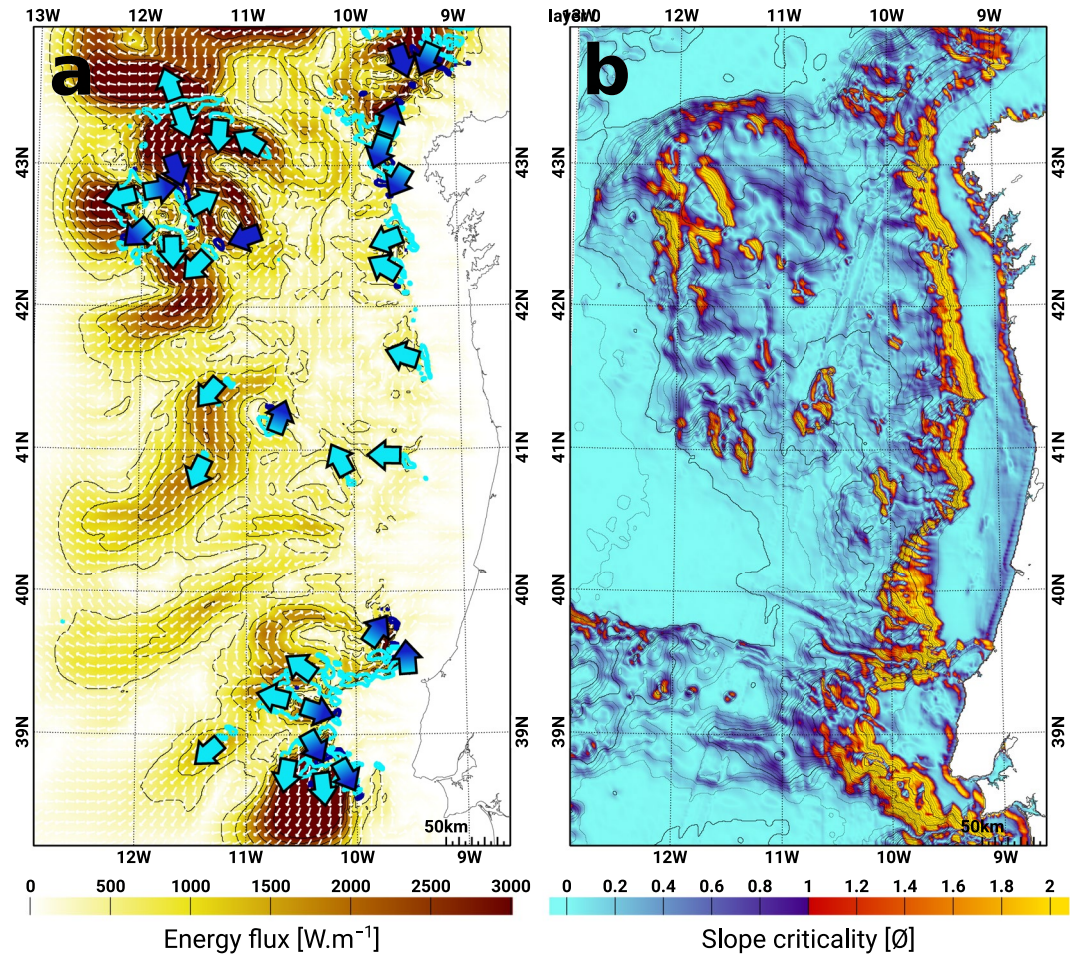


**Figure 3.** (a) Internal tide (IT) energy flux vertically integrated ( $\text{W}\cdot\text{m}^{-1}$ ) and conversion rate (cyan contours for generation and dark blue contours for sink). The cyan arrows refer to IT generation; the dark blue arrows refer to IT sinks, shading arrows refer to generated and locally dissipated ITs. (b) Ratio between the topography slope and the angle of the IT wave beam for diurnal tidal harmonics (based on M2). Values equal to 1 indicate critical slope areas; values  $<1$  refer to transmissive slopes (subcritical); and values  $>1$  refer to reflective slopes (supercritical).

where  $\rho$  is the sea water density,  $V_*$  is the friction velocity,  $C_D$  is the quadratic friction coefficient, and  $V$  is the velocity at the vertical mid-position of the bottom layer.  $C_D$  is calculated in BOBIBE simulation using the following equation:

$$C_D = \left( \frac{\kappa}{\ln\left(\frac{1}{z_0} \frac{h_b}{2}\right)} \right)^2 \quad (4)$$

where  $\kappa$  is the Von Karman constant ( $\kappa = 0.4$ ),  $z_0$  is the bottom roughness and  $h_b$  is the thickness of the bottom layer. Equation 4 is valid only if  $h_b$  is smaller than the height of the logarithmic velocity profile due to the bottom friction; a condition which is not met in the deep area of the domain. Thus,  $C_D$  is forced to be greater than  $2.5 \times 10^{-3}$  as it is commonly done in ocean modeling (Maraldi et al., 2013). The bottom roughness is the scale of unresolved topography at the sea floor, such as sand waves, ripples, or grain size. In the BOBIBE simulation,  $z_0 = 1 \times 10^{-3}$  m uniformly over the domain and corresponds to the order of roughness for continental slopes and abyssal plains.

To calculate the maximum  $\tau_b$  that could occur due to the tides, we calculated  $\mathbf{V}$  from the harmonic solutions of the simulation. A tidal prediction of  $\mathbf{V}$  from the simulated tidal harmonics (M2, S2, K1, and O1) is made over

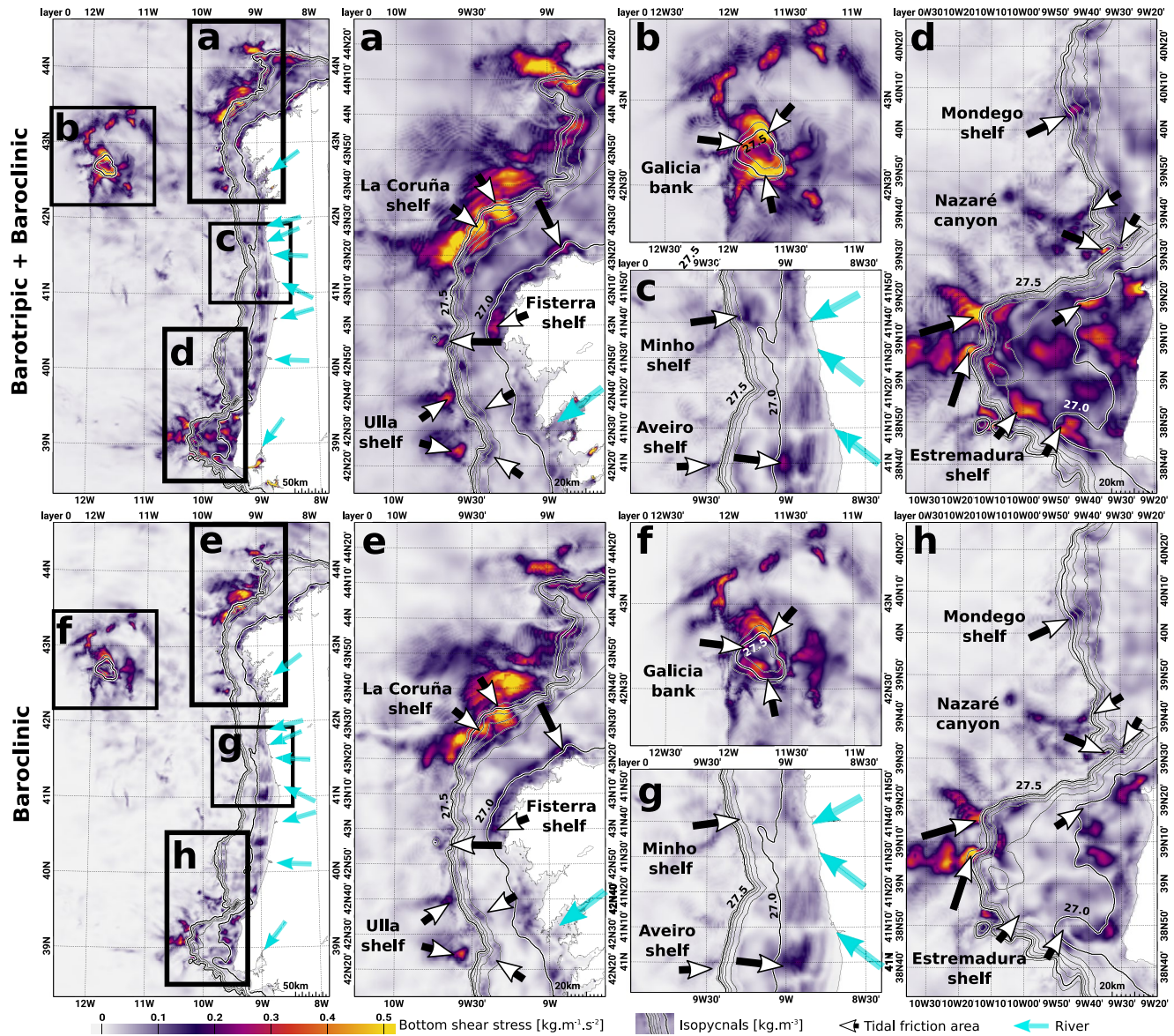


**Figure 4.** Total (top) and baroclinic (bottom) maximum tidal bottom shear stress from M2, S2, N2, K1, and O1 tidal harmonics over the Iberian continental shelf: (a, e) the northern shelf, (b, f) the Galicia Bank, (c, g) the central shelf and (d, h) the Southern shelf. The isopycnals reflect the potential density at the bottom and highlight the range of the GEOVIDE particle measurements (Figure 1). The black and white arrows highlight the potential areas of high bottom friction within the isopycnals range considered. The cyan arrows show the rivers bringing lithogenic particles and sediment.

2 months with a time resolution of 30 min. Then, the maximum of  $V$  is extracted from this prediction. This method was performed under two scenarios: the total tidal contribution (barotropic and baroclinic) and the baroclinic contribution only (Figure 4). Nine areas are selected where  $\tau_b > 0.1 \text{ kg.m}^{-1}.\text{s}^{-1}$ , within the range of isopycnals observed during the GEOVIDE cruise (black and white arrows in Figure 1). All areas are detailed below.

At the northern part of the Iberian Peninsula (Figures 4a and 4e), three areas show intense bottom friction. La Coruña shelf presents a wide area of strong bottom friction over the continental slope which partially corresponds to a critical slope. ITs are mainly generated and dissipated locally (Figure 3a) but also came from the cap further north ( $44.1^\circ\text{N}$ – $9^\circ\text{W}$ ) and from the Bay of Biscay. The Fisterra shelf presents a small sea mount within the continental slope which is crossed by the barotropic tides inducing a very localized bottom friction area. The bottom friction closer to the coast is more likely caused by the ITs from La Coruña shelf, dissipated on a critical slope. Then, the Ulla shelf presents two sites of ITs generation over critical slopes responsible for the bottom friction.

The Galicia Bank (Figures 4b and 4f) is a seamount with a summit at 800 m depth with ITs generated on most of its flanks. Other ITs are coming from other sea mounts further north, from the Bay of Biscay, and from the Iberian shelves. The maximum bottom friction locations correspond to critical slopes on the flanks of the sea mount but not over its top (Figure 3b).

At the central part (Figures 4c and 4g), Minho and Aveiro shelves are very similar, with barotropic tidal currents coming across steep slopes. But Minho bottom friction is only due to barotropic tides whereas Aveiro one involves ITs generated locally (Figures 3a and 4g). The maximum bottom friction over these areas is weaker than other sites and Aveiro bottom friction only partially corresponds to a critical slope.

Finally, at the southern part (Figures 4d and 4h), three other areas are highlighted. The Mondego shelf is influenced by the ITs from southern shelves, breaking over a supercritical slope. Even with a non-matching criticality, this area shows a medium bottom friction due to ITs. The Nazaré canyon presents ITs generation over its flanks with a strong bottom friction at the bottom of the canyon and some weaker over the northern flanks. These locations partially correspond to critical slopes. The Estremadura Spur shelf is highly influenced by barotropic tides and a lot of the bottom friction is only due to them (Figure 4h). ITs are generated at the western part over a complex bathymetry with many ITs dissipated locally (Figure 3a) over critical slopes.

To summarize, the simulation of ITs reveals nine areas with strong bottom friction that could generate sediment resuspension. Among them, three are over critical slopes, four others spread over both critical and not critical slopes and one occurs over supercritical slopes; one area is only due to barotropic tides so the slope criticality is not a concern. In this study, the criterion for sediment resuspension was the maximum tidal bottom friction therefore, the resuspension could occur following the spring-neap tide cycle. The fact that these areas do not strictly correspond to critical slopes increases the number of potential resuspension locations over shelves, offering new perspectives for worldwide sediment tidal resuspension investigations. Hereafter, all these selected areas will be referred to as tidal resuspension sites (TRS).

### 3.2. Sediment Resuspension Threshold

After identifying the potential TRS, we investigated whether bottom friction was strong enough to generate sediment resuspension at those sites. The threshold of sediment resuspension can be estimated using the static approach of the Shields criterion. Shields (1936) was one of the first to propose an empirical threshold of sediment resuspension in an adimensional space based on a lab experiment using multiple fluids and sediment. This methodology has been validated for the study of sediment motion in continental shelves by Larsen et al. (1981). This adimensional space uses the Shields parameter ( $\vartheta$ ) to compare bottom friction to sediment properties, and the boundary Reynolds number ( $Re_*$ ) to describe the turbulence of the flow at the scale of the sediment:

$$\vartheta = \frac{\tau_b}{gD(\rho_s - \rho)} \quad (5)$$

$$Re_* = V_* \frac{D}{\nu} = \sqrt{C_D} \frac{VD}{\nu} \quad (6)$$

where  $D$  is the grain diameter of the sediment,  $\rho$  is the density of the fluid,  $\rho_s$  is the dry bulk density of the sediment and  $\nu = 1.41 \times 10^{-6} \text{ m}^2 \cdot \text{s}^{-1}$  is the kinematic viscosity for sea water.

More recently, analytical Shields curves were formulated for various motion thresholds (motion, rolling, resuspension) and cohesive sediments (silts; Miedema, 2012a; 2012b, 2013). The curve for cohesive sediments has been chosen for the smallest grain size observed to be the most restrictive (7  $\mu\text{m}$ ), then the cohesive effect has been added to the rolling threshold. Because the parameters needed to properly generate these curves are missing, custom curves that fit the Shields curves were used.

The sediment properties at each potential TRS are found in the literature, from the closest in situ samples (Table 1). The sediment along the Iberian slope have a density from 2.3  $\text{g} \cdot \text{cm}^{-3}$  to 2.5  $\text{g} \cdot \text{cm}^{-3}$ , whereas the Galicia Bank sediment have a density of 1.7  $\text{g} \cdot \text{cm}^{-3}$  which greatly affect the relation between ( $D$ ,  $V$ ) and ( $\vartheta$ ,  $Re_*$ ). Thus, for clarity purposes, Galicia Bank is considered separately as well as the TRSs that present silt.

Figure 5 compares the values of  $\vartheta$  and  $Re_*$  at the potential TRS (colored rectangles) to the Shields curves (in black). Cases falling below the rolling curve correspond to steady sediment. Cases falling above the rolling curve



**Table 1**  
Characteristics of the Potential Tidal Resuspension Sites (TRS)

Area	Criticality	Isopycnals [ $\text{kg}\cdot\text{m}^{-3}$ ]	$\tau_b$ [ $\text{kg}\cdot\text{m}^{-1}\cdot\text{s}^{-2}$ ]	$\rho_s$ [ $\text{g}\cdot\text{cm}^{-3}$ ]	$D$ [ $\mu\text{m}$ ]	Nature	References	TRS
C	Yes/No	27.0–28.2	0.20–0.52	2.5	50–100	Lit.	Flach et al. (2002)	++
F	Yes	27.0–28.2	0.14–0.16	2.5	10–200	Lit.	van Weering and de Stigter (1998)	+
U	Yes	27.1–27.8	0.11–0.26	2.5	50–600	Mix.	van Weering and de Stigter (1998)	+
G	Yes/No	27.5	0.55–0.70	1.7	10–200	Bio.	Flach et al. (2002), Yenes et al. (2019)	++
Mi	Yes	27.1–27.2	0.23	2.3	150–500	Mix.	Dias and Nittrouer (1984)	0
A	Yes/No	27.1–27.8	0.28	2.3	10–300	Mix.	Dias and Nittrouer (1984)	+
M	No	27.0–27.5	0.25	2.3	60–500	Mix.	Dias and Nittrouer (1984), Duarte and Taborda (2007)	+
N	Yes/No	27.4–27.8	0.41	2.5	7–30	Lit.	de Stigter et al. (2007), Ribeiro (2008)	+
E	Yes	27.1–27.9	0.41	2.5	8–120	Mix.	Balsinha (2020)	++

Note. The flow dynamics at the bottom come from the IT simulation and the sediment properties come from the cited literature. The intensity of the sediment resuspension is symbolized by ++ when all the sediment can be resuspended, + when only the smaller fraction can and 0 when any of it can.

but below the resuspension curve correspond to lifted sediment which sink back. Cases falling above every curve are favorable to sediment resuspension, because the sediment is light enough, thin enough or the flow is strong enough (black labels in Figure 5a). Sediment with cohesive silt do not react the same as non-cohesive one so another curve is added for sediment with slits (Figures 5a and 5c).

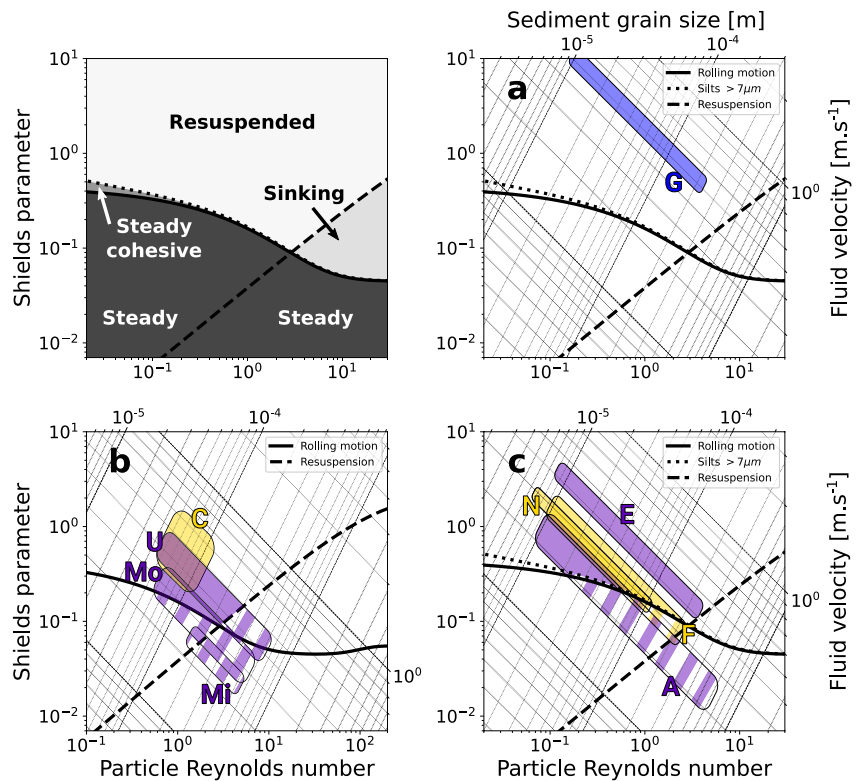


**Figure 5.** Sediment resuspension threshold for (a) silty light sediment tidal resuspension sites (TRSs), (b) dense sediment TRSs and (c) silty dense sediment TRSs. Above the solid line, the sediment is lifted from the sea floor, above the dotted line, the cohesive silts larger the  $7\mu\text{m}$  are lifted from the sea floor and above the dashed line the sediment stays in suspension. The colors denote the nature of the sediment: blue for biogenic, yellow for lithogenic, and purple for a mix of both. Hatched color highlights steady sediment. The grid scales of sediment grain size versus fluid velocity are computed for sea water properties ( $\nu = 1.10^{-3} \text{ m}^2\cdot\text{s}^{-1}$ ,  $\sigma = 27 \text{ kg}\cdot\text{m}^{-3}$ ) for sediment density  $\rho_s = 1.7 \text{ g}\cdot\text{cm}^{-3}$  (e.g., chalk) for (a) and  $\rho_s = 2.5 \text{ g}\cdot\text{cm}^{-3}$  (e.g., quartz, calcite) for (b, c).

The Galicia Bank, La Coruña shelf, and Estremadura Spur shelf are well above the threshold curve, suggesting that sediment resuspension occurs during the common tidal cycle. The Nazaré canyon and Fisterra shelf are mostly above the threshold curve, suggesting that only the finer fraction of the sediment is resuspended during the common tidal cycle and the medium fraction during spring tides. The Ulla, Aveiro, and Mondego shelves are crossed by the threshold, so only the finer fraction of the sediment can be resuspended during spring tides. The Minho shelf is way below the threshold, so the sediment size is too large and the flow too slow to generate sediment resuspension.

This method gives us a first order estimation of the TRS along the Iberian Peninsula. Table 1 summarizes the isopycnals, the nature of the sediment, and the intensity of the resuspension at the investigated TRS.

#### 4. Sediment Transport

As reported in the introduction, the suspended particles seem to be transported as far as 2,000 km offshore. However, IT transport of sediment only occurs over smaller scales (Masunaga et al., 2020; Molinas et al., 2020). In addition, ITs generated in the area do not present a significant propagation pattern that would allow connecting the stations 1, 13, or 21 (Figure 3a). Thus, we suggest that although ITs clearly trigger bottom friction and sediment resuspension, they are not responsible for the transport of suspended particles between the GEOVIDE stations; however, advection by the oceanic circulation may be. The IBIRYS operational reanalysis current field is used to investigate this transport. This product is a reanalysis from a 3D NEMO simulation at 1/12°: this simulation was assimilated with temperature and salinity profiles, sea surface height, and sea surface temperature to better represent the historical state of the ocean (further description and validation are provided by Maraldi et al., 2013). This simulation only extends to 19°W and therefore, does not include station 21 of the GEOVIDE cruise. The daily averaged currents of IBIRYS are collocated with GEOVIDE measurements for comparison. The measurements and simulation results have been found to be in agreement, asserting the use of this simulation to investigate the regional circulation (Figure S4 in Supporting Information S1).

The transport of the sediment by the circulation follow the isopycnals so IBIRYS have been interpolated at the isopycnals of the nepheloid layers observed:  $\sigma = 27.0, 27.17$  and  $27.39 \text{ kg.m}^{-3}$  (Figure 1). With a velocity range of  $3\text{--}10 \text{ cm.s}^{-1}$  and a distance between the TRS and the GEOVIDE stations of  $\sim 500 \text{ km}$ , the timescale involved ranges of 50–200 days. The monthly mean current field is averaged over three different time periods (2 yr, 6 and 3 months). For each period, the flow is considered steady and the streamlines are calculated to describe the potential pathways of the particles. When the shorter period is selected, a stronger mesoscale activity is observed with faster currents ( $\sim 10 \text{ cm.s}^{-1}$ ), whereas slower currents ( $\sim 3 \text{ cm.s}^{-1}$ ) are associated with the longer period. The sediment pathways from the TRS to the GEOVIDE stations slightly differ depending on the selected period; however, the general transport is clear. We choose to describe the sediment pathways using the 2 yr average (from June 2012 to June 2014) as it better shows a long-term mean state of the sediment transport (results based on the other periods are available in the Figure S5 in Supporting Information S1).

Figure 6 presents the streamlines from velocity fields at each isopycnals. Note that the current structures at  $27.0 \text{ kg.m}^{-3}$  (Figure 6a) are consistent with the surface circulation during the cruise (Zunino et al., 2017, their Figure 5, derived from altimetry sea level anomalies). Potential pathways from the TRS to the three GEOVIDE stations are inferred from the streamlines that connect them (colored arrows). The most striking feature is that no pathway directly connecting the three GEOVIDE stations is observed, at any isopycnal. A strong northward current along the shelf slope washes all the Iberian slope, and then splits up in different directions at La Coruña shelf. The potential pathways between each station are described and discussed below.

Station 1 is influenced by two eddies: in front of the Aveiro shelf, the eddy structure is found at the three isopycnals, whereas in front of the Nazaré canyon, the eddy only affects the shallower one. The TRS potentially affecting station 1 vary depending on the isopycnal: at  $27.0 \text{ kg.m}^{-3}$ , Aveiro, Mondego and Estremadura Spur TRSs (purple arrows, Figure 6a); at  $27.17 \text{ kg.m}^{-3}$ , Estremadura Spur TRS (purple arrow, Figure 6c); and at  $27.39 \text{ kg.m}^{-3}$ , Nazaré canyon and Estremadura Spur shelf (yellow and purple arrows, Figure 6c). With this method the station 1 seems mostly affected by mixed sediment so it can partially explain the lithogenic signature of the GEOVIDE observations. Note that some variations in the relative composition of the resuspended sediment cannot be excluded as well as other sediment coming from further south with the current as highlighted by Hernández-Molina et al. (2016).

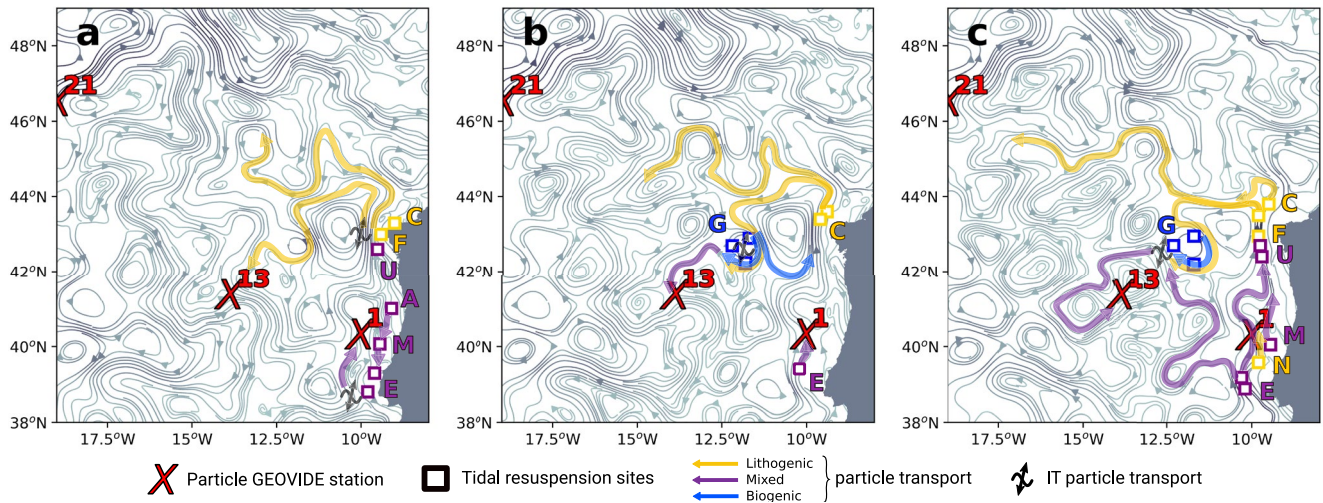


**Figure 6.** Streamline based on the mean velocity from June 2012 to June 2014 at (a)  $\sigma = 27.0 \text{ kg.m}^{-3}$ , (b)  $\sigma = 27.17 \text{ kg.m}^{-3}$  and (c)  $\sigma = 27.39 \text{ kg.m}^{-3}$ . The arrows describe the potential pathways of the particles that may link the tidal resuspension sites and the GEOVIDE stations. The colors define the nature of the particles transported: yellow for lithogenic, blue for biogenic, and purple for both lithogenic and biogenic. The internal tide (IT) symbol refers to a situation where the particles are transported across streamlines by ITs.

Station 13 is mostly influenced by southward and northeastward currents; thus, the lithogenic particles observed at this station are transported following a circuitous pathway. This pathway is the same at every isopycnals: starting from the La Coruña TRS and circumventing the Galicia Bank (Figure 6). At  $27.0 \text{ kg.m}^{-3}$ , this pathway transports particles mainly lithogenic from the La Coruña and Fisterra TRSs but also mixed sediment from Ulla TRS. At  $27.17$  and  $27.39 \text{ kg.m}^{-3}$  however, the resuspension of biogenic sediment at the Galicia Bank can completely invert the ratio of lithogenic/biogenic particle within the suspended particles (blue and yellow to purple arrows, Figures 6b and 6c). In addition, a current at  $27.39 \text{ kg.m}^{-3}$  seems to directly link Estremadura Spur TRS to station 13. Thus, we suggest that station 13 is affected by lithogenic particles for shallow isopycnals and mixed particles below. This is in good agreement with the GEOVIDE observations of lithogenic REEs (Figure 1).

Some streamlines seem to hardly connect the TRSs and the GEOVIDE station, but could if ITs transport the particles across the streamline over 50–100 km (IT symbols in Figure 6). This distance is comparable to that from the simulation of Masunaga et al. (2020), where the sediment is transported over 50 km by an IT flux of  $\sim 5 \text{ kW.m}^{-1}$  (their Figures 5 and 13f). This could happen near La Coruña/Fisterra shelf, Galicia Bank and Estremadura Spur shelf where ITs energy flux  $> 3 \text{ kW.m}^{-1}$  (Figure 3a). As for station 1, currents may also bring sediment from areas further south (Hernández-Molina et al., 2016).

Station 21 does not seem to connect with the TRS at any isopycnal. Long and meandering pathways could approach station 21 from La Coruña but no further than  $17^\circ\text{W}$  (yellow arrow, Figure 6c). Moreover, a large north-eastward current highly influences station 21: from  $\sim 12 \text{ cm.s}^{-1}$  at  $27.0 \text{ kg.m}^{-3}$  to  $6 \text{ cm.s}^{-1}$  at  $27.39 \text{ kg.m}^{-3}$ . This current is one of the southern branches of the North Atlantic Current (SNAC) highlighted by Zunino et al. (2017). The authors show that station 21 is under the influence of a large anticyclonic eddy during the cruise. This station displays very different temperatures and salinity than the nearby stations (Figure S1 in Supporting Information S1), with Subpolar Mode Water below 180 m and Subarctic Intermediate Water at 500 m (Garcia-Ibanez et al., 2018). Current velocity across the GEOVIDE transect highlights a strong shear current centered on station 21. It cannot be excluded that this complex circulation could bring water masses from other coastal/shelf margin locations than the Iberian coast. For example, the East North Atlantic Central Waters are highly represented at this depth (Garcia-Ibanez et al., 2018) and may have been influenced by ITs from the Gulf of Maine (Duda et al., 2018). The present choice of such regional model reanalysis does not enable us to reach a conclusion on the origins of the highly lithogenic particles observed at station 21. This will require further investigations based on a Lagrangian methodology (Artigue et al., 2020; Maes & Blanke, 2015) applied to a simulation of the North Atlantic basin reproducing the mixing of the various water masses in the North Atlantic and tidal dynamics. The ongoing study of neodymium isotopic composition (eNd) of the GEOVIDE samples could help to determine the exact origin of the particles (Grenier et al., 2018).

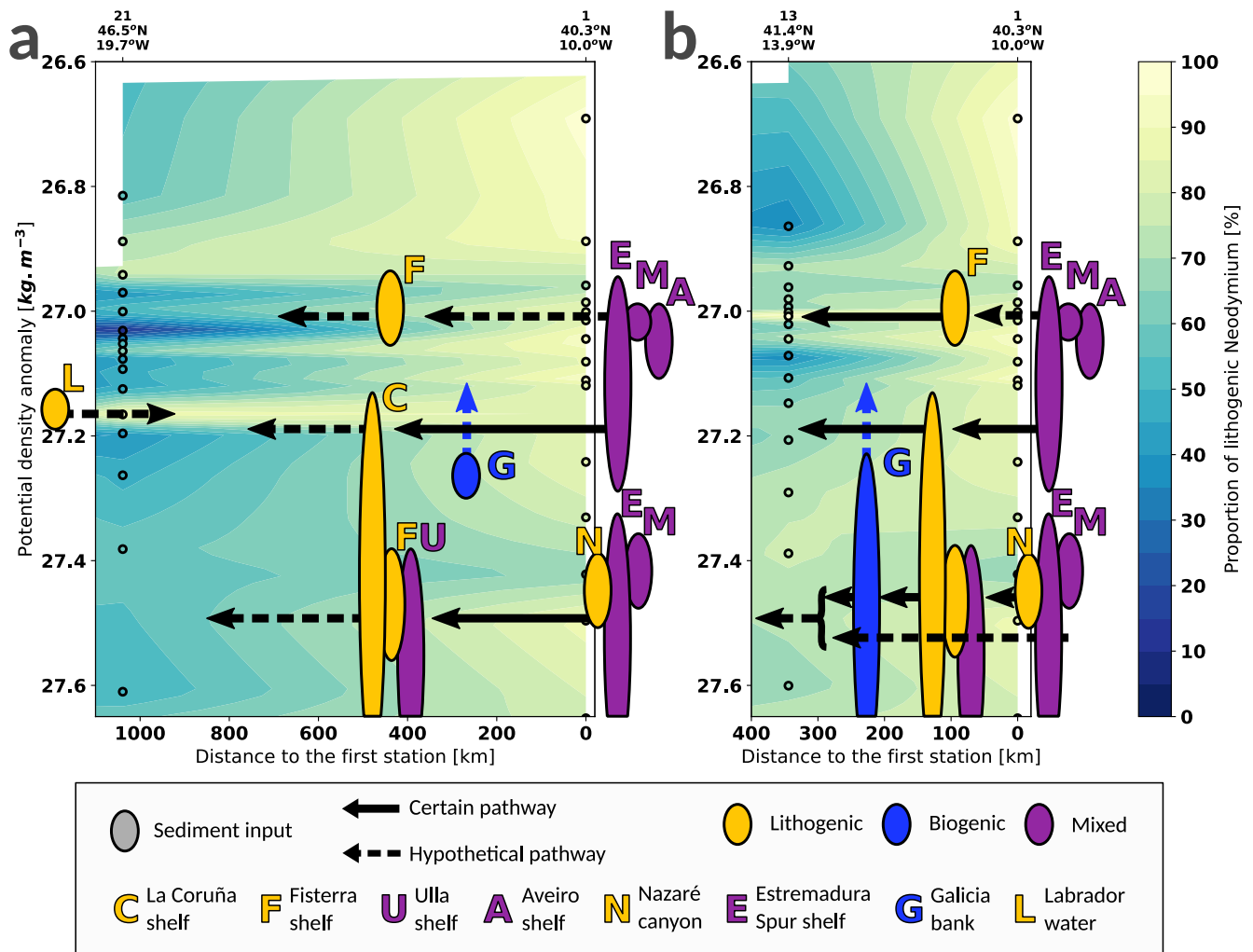


**Figure 7.** Proportion of lithogenic neodymium in particulate matter along isopycnals (a) between station 1 and 21 and (b) between station 1 and 13) using linear interpolation. The color inside the black rings refers to the GEOVIDE measurements. The other symbols refer to the tidal resuspension sites and the transport of the particles. On top of each station there is the station number and its localization. Data from Lagarde et al. (2020).

The simulation of the oceanic circulation provides a better understanding of the transport of the suspended particles over the area. Distinct pathways are highlighted for each station. Because stations 13 and 21 are not connected, the interpolation of the particulate lithogenic fraction between these two stations is not relevant and hampers the interpretation of the results. Distinct interpolations of the GEOVIDE measurements are proposed in Figure 7. The results shown in Table 1 and Figure 6 were added to Figure 7 in order to propose a clear summary of our study.

## 5. Conclusion and Perspectives

This study proposes the first interdisciplinary approach to explain the resuspension and transport of lithogenic particles from the Iberian coast to the middle of the North Atlantic basin. Based on a semi-realistic 3D tidal model and sediment properties, we establish that ITs generated in the Bay of Biscay and along the Iberian slope participate in sediment resuspension and could be the major mechanism for the resuspension occurring below 300 m. Eight TRS are identified: La Coruña shelf, Fisterra shelf and Nazaré canyon are sources of lithogenic sediment, the Ulla, Aveiro, Mondego and Estremadura Spur shelves are likely providing both lithogenic and biogenic sediments, and the Galicia Bank is a source of biogenic sediment. Most of these sites are under strong IT influence, except some areas of Estremadura Spur shelf, strong bottom friction is only due to barotropic tidal currents at the top of the shelf slope. Using a regional model reanalysis, the mean state of the oceanic circulation

in the area is investigated on the suspected isopycnals. Associated with the TRS, this approach explains most of the GEOVIDE observations (Lagarde et al., 2020). However, we demonstrate that stations 13 and 21 are not connected. More specifically, the significant lithogenic fraction and the water masses observed at station 21 at 500 m ( $27.17 \text{ kg}\cdot\text{m}^{-3}$ ) could reflect transport of sediment originating from the North American margins rather than from the Iberian margin.

More broadly, questions raised by the geochemical results lead to the development of this method associating dedicated IT simulation to regional circulation one. This strategy helped to improve the first interpretations of the geochemical data (Gourain et al., 2019; Lagarde et al., 2020). Not all TRS from this study are located on critical slopes, and many critical slopes of the Iberian Peninsula are not associated with a TRS. Thus, we suggest that the slope criticality is not sufficient to properly identify TRS and should be reserved to internal solitary waves (in the upper 300 m). An explicit modeling of the ITs with a thin grid resolution ( $<3 \text{ km}$ ) and a good knowledge of the sediment properties (nature and size) are required to simulate and identify TRSs. Further work on sediment resuspension and large distance particle transport should consider applying Lagrangian tracking to the oceanic circulation simulations as well as performing a complete tidal-circulation model coupled with a sediment model.

### Data Availability Statement

The GEOVIDE CTD data are available at SENOE (DOI: [10.17882/52153](https://doi.org/10.17882/52153)). The GEOVIDE geochemical tracer data and OMEX II-II sediment data are available at BODC (<https://www.bodc.ac.uk/geotraces/data/idp2017/>; <https://www.bodc.ac.uk/omex/omexii-ii/>). FES2014b tidal atlas is available at SEDOO (DOI: [10.6096/3001](https://doi.org/10.6096/3001)). IBIRYS12 is available at CMEMS (DOI: [10.48670/moi-00029](https://doi.org/10.48670/moi-00029)).

### References

- Artigue, L., Lacan, F., Van Gennip, S., Lohan, M. C., Wyatt, N. J., Woodward, E. M. S., et al. (2020). Water mass analysis along  $22^{\circ}\text{N}$  in the subtropical North Atlantic for the JC150 cruise (Geotraces, GApr08). *Deep Sea Research Part I: Oceanographic Research Papers*, 103230.
- Balsinha, M. J. (2020). *Sedimentary dynamics in the Estremadura Spur continental shelf*, (Unpublished doctoral dissertation). Universidade de Lisboa.
- Boegman, L., & Stastna, M. (2019). Sediment resuspension and transport by internal solitary waves. *Annual Review of Fluid Mechanics*, 51, 129–154. <https://doi.org/10.1146/annurev-fluid-122316-045049>
- Buijsman, M. C., Arbic, B. K., Richman, J. G., Shriver, J. F., Wallcraft, A. J., & Zamudio, L. (2017). Semidiurnal internal tide incoherence in the equatorial Pacific. *Journal of Geophysical Research: Oceans*, 122(7), 5286–5305. <https://doi.org/10.1002/2016jc012590>
- Cacchione, D. (1970). *Experimental study of internal gravity waves over a slope*, (Unpublished doctoral dissertation). Massachusetts Institute of Technology and Woods Hole Oceanographic Institution.
- Cacchione, D., Pratson, L. F., & Ogston, A. (2002). The shaping of continental slopes by internal tides. *Science*, 296(5568), 724–727. <https://doi.org/10.1126/science.1069803>
- de Lavergne, C., Falahat, S., Madec, G., Roquet, F., Nycander, J., & Vic, C. (2019). Toward global maps of internal tide energy sinks. *Ocean Modeling*, 137, 52–75. <https://doi.org/10.1016/j.ocemod.2019.03.010>
- de Madron, X. D., Castaing, P., Nyffeler, F., & Courp, T. (1999). Slope transport of suspended particulate matter on the Aquitanian margin of the Bay of Biscay. *Deep Sea Research Part II: Topical Studies in Oceanography*, 46(10), 2003–2027.
- de Stigter, H. C., Boer, W., de Jesus Mendes, P. A., Jesus, C. C., Thomsen, L., van den Bergh, G. D., & van Weering, T. C. (2007). Recent sediment transport and deposition in the Nazaré Canyon, Portuguese continental margin. *Marine Geology*, 246(2–4), 144–164. <https://doi.org/10.1016/j.margeo.2007.04.011>
- Dias, J., Jouanneau, J., Gonzalez, R., Araújo, M., Drago, T., Garcia, C., et al. (2002). Present day sedimentary processes on the northern Iberian shelf. *Progress in Oceanography*, 52(2–4), 249–259. [https://doi.org/10.1016/s0079-6611\(02\)00009-5](https://doi.org/10.1016/s0079-6611(02)00009-5)
- Dias, J., & Nittrouer, C. A. (1984). Continental shelf sediments of northern Portugal. *Continental Shelf Research*, 3(2), 147–165.
- Duarte, J. F., & Taborda, R. (2007). Bottom sediment signature associated with the Oporto, Aveiro, and Nazaré Submarine Canyons (NW off Portugal). *Thalassia*, 23(1), 9–18.
- Duda, T. F., Lin, Y.-T., Buijsman, M., & Newhall, A. E. (2018). Internal tidal modal ray refraction and energy ducting in baroclinic Gulf Stream currents. *Journal of Physical Oceanography*, 48(9), 1969–1993. <https://doi.org/10.1175/jpo-d-18-0031.1>
- Estournel, C., Marsaleix, P., & Ulses, C. (2021). A new assessment of the circulation of Atlantic and intermediate waters in the eastern Mediterranean. *Progress in Oceanography*, 198, 102673. <https://doi.org/10.1016/j.pocean.2021.102673>
- Flach, E., Muthumbi, A., & Heip, C. (2002). Meiofauna and macrofauna community structure in relation to sediment composition at the Iberian margin compared to the Goban Spur (NE Atlantic). *Progress in Oceanography*, 52(2–4), 433–457. [https://doi.org/10.1016/s0079-6611\(02\)00018-6](https://doi.org/10.1016/s0079-6611(02)00018-6)
- Garcia-Ibanez, M. I., Pérez, F. F., Lherminier, P., Zunino, P., Mercier, H., & Tréguer, P. (2018). Water mass distributions and transports for the 2014 GEOVIDE cruise in the North Atlantic. *Biogeosciences*, 15(7), 2075–2090. <https://doi.org/10.5194/bg-15-2075-2018>
- Garrett, C., & Kunze, E. (2007). Internal tide generation in the deep ocean. *Annual Review of Fluid Mechanics*, 39, 57–87. <https://doi.org/10.1146/annurev.fluid.39.050905.110227>
- Gourain, A., Planquette, H., Cheize, M., Lemaitre, N., Menzel Barraqueta, J.-L., Shelley, R., et al. (2019). Inputs and processes affecting the distribution of particulate iron in the North Atlantic along the GEOVIDE (GEOTRACES GA01) section. *Biogeosciences*, 16(7), 1563–1582. <https://doi.org/10.5194/bg-16-1563-2019>

### Acknowledgments

The authors are grateful to the CNES, CLS, CNRS, and UPS for the funding of this study. The authors are thankful to D. Allain for the development of the POCViP visualization software, to H. de Stigter, who provided us with the sediment properties near the Nazaré canyon, and to R. Almar for his advice on sediment resuspension. The BOBIBE simulation was performed using HPC resources from GENCI/CINES (Grants 2020-A0080110098 and 2021A0100110098). The GEOVIDE geochemical tracer data, as part of GEOTRACE program, are provided by the British Oceanographic Data Centre (BODC), funded by the Scientific Committee on Oceanic Research, the US National Science Foundation, and the UK Natural Environment Research Council. The sediment properties from OMEX II-II project are provided by the BODC, funded by the European Commission through the Marine Science and Technology program.

- Grenier, M., Garcia-Solsona, E., Lemaitre, N., Trull, T. W., Bouvier, V., Nonnotte, P., et al. (2018). Differentiating lithogenic supplies, water mass transport, and biological processes on and off the Kerguelen Plateau using rare Earth element concentrations and neodymium isotopic compositions. *Frontiers in Marine Science*, 5, 426. <https://doi.org/10.3389/fmars.2018.00426>
- Hernández-Molina, F. J., Wåhlin, A., Bruno, M., Ercilla, G., Llave, E., Serra, N., et al. (2016). Oceanographic processes and morphosedimentary products along the Iberian margins: A new multidisciplinary approach. *Marine Geology*, 378, 127–156. <https://doi.org/10.1016/j.margeo.2015.12.008>
- Huthnance, J. (1989). Internal tides and waves near the continental shelf edge. *Geophysical & Astrophysical Fluid Dynamics*, 48(1–3), 81–106. <https://doi.org/10.1080/03091928908219527>
- Huthnance, J., Van Aken, H. M., White, M., Barton, E. D., Le Cann, B., Coelho, E. F., et al. (2002). Ocean margin exchange—Water flux estimates. *Journal of Marine Systems*, 32(1–3), 107–137. [https://doi.org/10.1016/s0924-7963\(02\)00034-9](https://doi.org/10.1016/s0924-7963(02)00034-9)
- Jia, Y., Tian, Z., Shi, X., Liu, J. P., Chen, J., Liu, X., et al. (2019). Deep-sea sediment resuspension by internal solitary waves in the northern South China Sea. *Scientific Reports*, 9(1), 1–8. <https://doi.org/10.1038/s41598-019-47886-y>
- Lagarde, M., Lemaitre, N., Planquette, H., Grenier, M., Belhadj, M., Lherminier, P., & Jeandel, C. (2020). Particulate rare Earth element behavior in the North Atlantic (GEOVIDE cruise). *Biogeosciences*. <https://doi.org/10.5194/bg-17-5539-2020>
- Lam, P. J., Heller, M. I., Lerner, P. E., Moffett, J. W., & Buck, K. N. (2020). Unexpected source and transport of iron from the deep Peru margin. *ACS Earth and Space Chemistry*, 4(7), 977–992. <https://doi.org/10.1021/acsearthspacechem.0c00066>
- Larsen, L., Sternberg, R., Shi, N., Marsden, M., & Thomas, L. (1981). Field investigations of the threshold of grain motion by ocean waves and currents. *Marine Geology*, 42(1–4), 105–132. [https://doi.org/10.1016/s0070-4571\(08\)70296-6](https://doi.org/10.1016/s0070-4571(08)70296-6)
- Lyard, F. H., Allain, D. J., Cancet, M., Carrère, L., & Picot, N. (2021). FES2014 global ocean tides atlas: Design and performances. *Ocean Science Discussions*, 2021, 1–40. <https://doi.org/10.5194/os-2020-96>
- Maes, C., & Blanke, B. (2015). Tracking the origins of plastic debris across the Coral Sea: A case study from the Ouvéa Island, New Caledonia. *Marine Pollution Bulletin*, 97(1), 160–168. <https://doi.org/10.1016/j.marpolbul.2015.06.022>
- Maraldí, C., Chanut, J., Levier, B., Ayoub, N., Mey, P. D., Reffray, G., et al. (2013). NEMO on the shelf: Assessment of the Iberia-Biscay-Ireland configuration. *Ocean Science*, 9(4), 745–771. <https://doi.org/10.5194/os-9-745-2013>
- Marin, F. (2011). Solitons: Historical and physical introduction. In R. A. Meyers (Ed.), *Mathematics of complexity and dynamical systems* (pp. 1561–1575). Springer New York. [https://doi.org/10.1007/978-1-4614-1806-1\\_100](https://doi.org/10.1007/978-1-4614-1806-1_100)
- Marsaleix, P., Auclair, F., Floor, J. W., Herrmann, M. J., Estournel, C., Pairaud, I., & Ulses, C. (2008). Energy conservation issues in sigma-coordinate free-surface ocean models. *Ocean Modeling*, 20(1), 61–89. <https://doi.org/10.1016/j.ocemod.2007.07.005>
- Marsaleix, P., Michaud, H., & Estournel, C. (2019). 3D phase-resolved wave modeling with a non-hydrostatic ocean circulation model. *Ocean Modeling*, 136, 28–50. <https://doi.org/10.1016/j.ocemod.2019.02.002>
- Masunaga, E., Arthur, R. S., Fringer, O. B., & Yamazaki, H. (2017). Sediment resuspension and the generation of intermediate nepheloid layers by shoaling internal bores. *Journal of Marine Systems*, 170, 31–41. <https://doi.org/10.1016/j.jmarsys.2017.01.017>
- Masunaga, E., Arthur, R. S., & Yamazaki, H. (2020). Baroclinic residual circulation and mass transport due to internal tides. *Journal of Geophysical Research: Oceans*, 125(4), e2019JC015316. <https://doi.org/10.1029/2019jc015316>
- McCave, I., & Hall, I. R. (2002). Turbidity of waters over the northwest Iberian continental margin. *Progress in Oceanography*, 52(2–4), 299–313. [https://doi.org/10.1016/s0079-6611\(02\)00012-5](https://doi.org/10.1016/s0079-6611(02)00012-5)
- Miedema, S. (2012a). Constructing the shields curve. Part A: Fundamentals of the sliding, rolling, and lifting mechanisms for the entrainment of particles. *Journal of Dredging Engineering*, 12(1), 1–49.
- Miedema, S. (2012b). Constructing the shields curve. Part B: Sensitivity analysis, exposure and protrusion levels settling velocity, shear stress and friction velocity, erosion flux and laminar main flow. *Journal of Marine Science and Engineering*, 12, 50–92.
- Miedema, S. (2013). Constructing the shields curve. Part C: Cohesion by silt, Hjulstrom, Sundborg. *International Conference on Offshore Mechanics and Arctic Engineering*, 55409, V006T10A023
- Molinas, E., Carneiro, J. C., & Vinzon, S. (2020). Internal tides as a major process in Amazon continental shelf fine sediment transport. *Marine Geology*, 430, 106360. <https://doi.org/10.1016/j.margeo.2020.106360>
- Oliveira, A., Vitorino, J., Rodrigues, A., Jouanneau, J., Dias, J., & Weber, O. (2002). Nepheloid layer dynamics in the northern Portuguese shelf. *Progress in Oceanography*, 52(2–4), 195–213. [https://doi.org/10.1016/s0079-6611\(02\)00006-x](https://doi.org/10.1016/s0079-6611(02)00006-x)
- Pairaud, I. L., Auclair, F., Marsaleix, P., Lyard, F., & Pichon, A. (2010). Dynamics of the semi-diurnal and quarter-diurnal internal tides in the Bay of Biscay. Part 2: Baroclinic tides. *Continental Shelf Research*, 30(3–4), 253–269. <https://doi.org/10.1016/j.csr.2009.10.008>
- Pairaud, I. L., Lyard, F., Auclair, F., Letellier, T., & Marsaleix, P. (2008). Dynamics of the semi-diurnal and quarter-diurnal internal tides in the Bay of Biscay. Part 1: Barotropic tides. *Continental Shelf Research*, 28(10–11), 1294–1315. [10.1016/j.csr.2008.03.004](https://doi.org/10.1016/j.csr.2008.03.004)
- Puig, P., Palanques, A., Guillén, J., & El Khatib, M. (2004). Role of internal waves in the generation of nepheloid layers on the northwestern Alboran slope: Implications for continental margin shaping. *Journal of Geophysical Research: Oceans*, 109(C9). <https://doi.org/10.1029/2004jc002394>
- Quaresma, L. S., Vitorino, J., Oliveira, A., & da Silva, J. (2007). Evidence of sediment resuspension by nonlinear internal waves on the western Portuguese mid-shelf. *Marine Geology*, 246(2–4), 123–143. <https://doi.org/10.1016/j.margeo.2007.04.019>
- Ribbe, J., & Holloway, P. E. (2001). A model of suspended sediment transport by internal tides. *Continental Shelf Research*, 21(4), 395–422. [https://doi.org/10.1016/s0278-4343\(00\)00081-9](https://doi.org/10.1016/s0278-4343(00)00081-9)
- Ribeiro, M. (2008). *Dinâmica sedimentar da cabeceira do canhão submarino da nazaré* (p. 14). Faculdade de Ciências da Universidade de Lisboa.
- Schmidt, S., Chou, L., & Hall, I. R. (2002). Particle residence times in surface waters over the north-western Iberian margin: Comparison of pre-upwelling and winter periods. *Journal of Marine Systems*, 32(1–3), 3–11. [https://doi.org/10.1016/s0924-7963\(02\)00027-1](https://doi.org/10.1016/s0924-7963(02)00027-1)
- Shields, A. (1936). *Anwendung der aehnlichkeitsmechanik und der turbulenzforschung auf die geschiebewegung*, (Ph.D. thesis). Technical University.
- Toublanc, F., Ayoub, N., Lyard, F., Marsaleix, P., & Allain, D. (2018). Tidal downscaling from the open ocean to the coast: A new approach applied to the Bay of Biscay. *Ocean Modeling*, 124, 16–32. <https://doi.org/10.1016/j.ocemod.2018.02.001>
- van Weering, T. C., & de Stigter, H. C. (1998). *Benthic boundary layer forcing on Iberian margin particle fluxes and accumulation* (Tech. Rep.). OMEX II-II Second Annual Science Report. Retrieved from [https://www.bodc.ac.uk/omex/omexii-ii/report/05a\\_sr.pdf](https://www.bodc.ac.uk/omex/omexii-ii/report/05a_sr.pdf)
- Van Weering, T. C., De Stigter, H., Boer, W., & De Haas, H. (2002). Recent sediment transport and accumulation on the NW Iberian margin. *Progress in Oceanography*, 52(2–4), 349–371. [https://doi.org/10.1016/s0079-6611\(02\)00015-0](https://doi.org/10.1016/s0079-6611(02)00015-0)
- Yenes, M., Casas, D., Nespereira, J., Monterrubio, S., Ercilla, G., & López-González, N. (2019). Galicia bank sediment transport activity in response to continuous sedimentary instability dynamics: A geotechnical perspective. *International Journal of Earth Sciences*, 108(8), 2545–2560. <https://doi.org/10.1007/s00531-019-01776-w>

- Zaron, E. D. (2019). Baroclinic tidal sea level from exact-repeat mission altimetry. *Journal of Physical Oceanography*, *49*(1), 193–210. <https://doi.org/10.1175/JPO-D-18-0127.1>
- Zunino, P., Lherminier, P., Mercier, H., Daniault, N., García-Ibáñez, M. I., & Pérez, F. F. (2017). The GEOVIDE cruise in May–June 2014 reveals an intense meridional overturning circulation over a cold and fresh subpolar North Atlantic. *Biogeosciences*, *14*(23), 5323–5342. <https://doi.org/10.5194/bg-14-5323-2017>

## References From the Supporting Information

- Arakawa, A., & Lamb, V. R. (1981). A potential enstrophy and energy conserving scheme for the shallow water equations. *Monthly Weather Review*, *109*(1), 18–36. [https://doi.org/10.1175/1520-0493\(1981\)109<0018:apeaec>2.0.co;2](https://doi.org/10.1175/1520-0493(1981)109<0018:apeaec>2.0.co;2)
- Costa, A., Doglioli, A. M., Marsaleix, P., & Petrenko, A. A. (2017). Comparison of in situ microstructure measurements to different turbulence closure schemes in a 3D numerical ocean circulation model. *Ocean Modeling*, *120*, 1–17. <https://doi.org/10.1016/j.ocemod.2017.10.002>
- Damien, P., Bosse, A., Testor, P., Marsaleix, P., & Estournel, C. (2017). Modeling postconvective submesoscale coherent vortices in the north-western Mediterranean Sea. *Journal of Geophysical Research: Oceans*, *122*(12), 9937–9961. <https://doi.org/10.1002/2016jc012114>
- Grebenkov, D. S., & Serror, J. (2014). Following a trend with an exponential moving average: Analytical results for a Gaussian model. *Physica A: Statistical Mechanics and Its Applications*, *394*, 288–303. <https://doi.org/10.1016/j.physa.2013.10.007>
- Griffies, S. M., & Hallberg, R. W. (2000). Biharmonic friction with a Smagorinsky-like viscosity for use in large-scale eddy-permitting ocean models. *Monthly Weather Review*, *128*(8), 2935–2946. [https://doi.org/10.1175/1520-0493\(2000\)128<2935:bfwasl>2.0.co;2](https://doi.org/10.1175/1520-0493(2000)128<2935:bfwasl>2.0.co;2)
- Jackett, D. R., McDougall, T. J., Feistel, R., Wright, D. G., & Griffies, S. M. (2006). Algorithms for density, potential temperature, conservative temperature, and the freezing temperature of sea water. *Journal of Atmospheric and Oceanic Technology*, *23*(12), 1709–1728. <https://doi.org/10.1175/jtech1946.1>
- Kundu, P., Cohen, M. I., & Hu, H. H. (2004). *Fluid mechanics*. Elsevier Academic Press.
- Leonard, B. P. (1979). A stable and accurate convective modeling procedure based on quadratic upstream interpolation. *Computer Methods in Applied Mechanics and Engineering*, *19*(1), 59–98. [https://doi.org/10.1016/0045-7825\(79\)90034-3](https://doi.org/10.1016/0045-7825(79)90034-3)
- Marsaleix, P., Auclair, F., & Estournel, C. (2006). Considerations on open boundary conditions for regional and coastal ocean models. *Journal of Atmospheric and Oceanic Technology*, *23*(11), 1604–1613. <https://doi.org/10.1175/jtech1930.1>
- Marsaleix, P., Auclair, F., & Estournel, C. (2009). Low-order pressure gradient schemes in sigma coordinate models: The seamount test revisited. *Ocean Modeling*, *30*(2–3), 169–177. <https://doi.org/10.1016/j.ocemod.2009.06.011>
- Siddorn, J., & Furner, R. (2013). An analytical stretching function that combines the best attributes of geopotential and terrain-following vertical coordinates. *Ocean Modeling*, *66*, 1–13. <https://doi.org/10.1016/j.ocemod.2013.02.001>